Research Article
Hittite Journal of Science and Engineering, 2023, 10 (3) 259–267
ISSN NUMBER: 2148–4171
DOI: 10.17350/HJSE19030000315

On The Blind Denoising Efficiency of Image Denoising Algorithms Through Robustness, Image Quality and Computational Burden

Kenan Gencol
Hitit University, Department of Electrical and Electronics Engineering, Corum, Türkiye

ABSTRACT

The main goal of the image denoising is to recover the original image while attaining the structure of the image as much as possible. When the image denoising task is blind, we have no a priori information about the original image. Thus, we cannot measure the degradation level in the image directly; instead, noise variance can be estimated by the denoising algorithm. According to the estimated value, denoising is performed. Such algorithms are supposed to be robust to varying and high levels of noise interference. Moreover, in time-constrained real-world applications, they must balance the tradeoff between image quality and computation time. In this study, we assess the performance of the image denoising algorithms armored for these goals. We are aimed to determine the optimal performance yielded by such algorithms and the noise bounds wherein each algorithm is superior. After the experimental work, important conclusions are drawn.

Keywords:
Image processing; Image analysis; Image denoising; Filtering; Noise

Article History:
Received: 2023/05/26
Accepted: 2023/09/13
Online: 2023/09/30

***Correspondence to**: Kenan Gencol, Hitit University, Electrical and Electronics Engineering, 19030, Corum, TÜRKİYE*
E-Mail: kenangencol@hitit.edu.tr;
Phone: +90 364 219 1302;
Fax: +90 364 219 1399.

This article has been checked for similarity.

INTRODUCTION

Let $s(t)$ be a reference signal corrupted by additive white Gaussian noise (AWGN), i.e, $sN(t) = s(t) + w(t)$ where $w(t) \sim N(0, a^2)$ is AWGN with zero mean and a^2 variance. When $s(t)$ is considered to be an image signal, the main goal of image denoising is to recover signal $s(t)$ while preserving image structures and features as much as possible. In the process of recovering original signal, the suppression of noise and preservation of image details is a compromise. Noise can be due to imperfections in camera sensory systems and imaging process, different sources of noise such as photon, thermal and quantization noise, poor illumination conditions, etc.

One of the oldest and simplest methods of denoising is to average the image spatially. This process acts as a low-pass filter and removes the noise by smoothing it. In smoothing operations, the pixels that have significantly higher or lower intensity values would smear across neighboring pixels and thus create blur. Similarly, neighborhood filters which take an input pixel and apply an algorithm to neighbor pixels of the corresponding pixel create shocks and artifacts [1,2]. To address the blurring problems of spatial and neighborhood filters anisotropic diffusion filter [3] was designed by Perona and Malik to avoid the blurring effects of spatial and neighborhood filters. This filter smooths the image in the direction that is orthogonal to the gradient direction. Also, a minimization technique called total variation filter [4] designed by Rudin et al. acts for the same goal. Unfortunately, these two approaches are fairly slow and come with more computation burden compared to aforementioned spatial techniques. It is a fact that noise commonly manifests itself as fine grained structure in images. Many researches have been conducted addressing this phenomenon. Wavelet based techniques [5-7] rely on this phenomenon. In wavelet domain, most of the noise is represented by wavelet coefficients at finer scales. The coefficients are thresholded to get rid of unwanted noise. The main handicap of wavelet thresholding techniques is that the chosen threshold may not match the specific distribution of image signal. Also, hard thresholding would create visual artifacts and soft thresholding would create blur in the recovered image. Nonlinear estimators based on Bayesian theory attempt to overcome the disadvantages of wavelet based methods at cost of high computation burden [8]. On the other hand, an algorithm called Non-Local Means [9-10] brought a new perspective to image denoising task. This algorithm have for the first time used patch-wise pixel

operations instead of point-wise pixel operations. As a second contribution, the algorithm has considered the patches physically not near the pixel of interest and hence having its name as nonlocal. Following this, the search for optimally designing a filter that maximizes the signal-to-noise ratio (SNR) for each component of the signal in Wiener filter resulted an algorithm that is still considered as the state-of-the-art called Block-Matching and 3-D Filtering (BM3D) [11]. This algorithm stacks the 2-D noisy image patches into 3-D groups and then a high-dimensional filtering approach called collaborative filtering is employed. This latter operation includes 3-D transform, shrinkage and inverse transform of image data. Recently, some image denoising techniques based on deep learning appear [12]. But, these methods need lots of data for training and are not yet mature to be employed in real-world denoising operations. Interested readers can refer to [13] for more comprehensive review of the image denoising algorithms.

The remainder of the paper is organized as follows. In the next section, the algorithms suitable for blind image denoising are briefly explained. Then, the results obtained on the basis of quality, robustness and computation time are presented and discussed. Finally, some concluding remarks are given.

MATERIAL AND METHODS

In this section, we introduce the problem of image denoising and briefly explain the algorithms suitable for blind image denoising. Gaussian, Wiener, NLM, Wavelet hard and soft denoising methods, and BM3D are evaluated and the results are presented in terms of image quality metrics and computational efficiency.

Problem Definition

Let the problem be modeled as

$$y(i,j) = x(i,j) + n(i,j) \tag{1}$$

where *x(i, j)* is the noise-free input image, $n(i, j) \sim N(0, \sigma^2)$ is AWGN and y(i, j) is the noisy image observed. We would like to obtain an estimate $\hat{x}$ of the original image, *x*. A relatively simple approach is to convolve (or correlate) the noisy image with a lowpass kernel centered at *(i, j)* in spatial domain, i.e,

$$\hat{x} = y * h \tag{2}$$

where $\hat{x}$ is the estimate of noise-free image and h is the NxN kernel with weights satisfying the general rule: $\sum w(i, j) = 1$. The simplest weighted averaging filter is the average (or smoothing) filter with weights 1/(*NxN*), 2-D, an isotropic (i.e, circularly symmetric) Gaussian filter [14] has the form:

$$w(i,j,k,l) = w(|i-k|,|j-l|) = \frac{1}{\sum_{k,l} w(i,j,k,l)} e^{-(|i-k|^2+|j-l|^2)} \tag{3}$$

Wiener Filter

In wiener filtering, the goal is to obtain a linear estimate of the noise-free image, $\hat{x}(i, j)$ of the size MxN that minimizes the mean squared error (MSE), i.e.

$$MSE = \frac{1}{MN} \sum_{i,j=1}^{i,j=M,N} (\hat{x}(i,j) - x(i,j))^2 \tag{4}$$

This linear estimate is given by

$$\hat{x}(i,j) = \frac{\sigma_x^2(i,j)}{\sigma_x^2(i,j) + \sigma_n^2(i,j)} [y(i,j) - \mu_x(i,j)] + \mu_x(i,j) \tag{5}$$

where σ_x^2 and μ_x are the signal variance and the mean of the original image and σ_n^2 is the variance of noise, respectively. The wiener filter is optimal when *x(i, j)* and *n(i, j)* are stationary Gaussian processes.

Non-local Means (NLM)

The NLM method aims to take advantage of the high degree of redundancy found in any natural images. It uses the fact that every small window in a natural image has many similar windows in the same image:

$$NL[x](i) = \sum_{j \in I} w(i,j) v(j) \tag{6}$$

where weighting kernel *w(i, j)* depends on the similarity between the pixels *i* and *j*:

$$w(i,j) = \frac{1}{Z(i)} e^{\frac{\|v(N_i) - v(N_j)\|^2}{h^2}} \tag{7}$$

and *Z(i)* is the normalizing constant:

$$Z(i) = \sum_i e^{\frac{\|v(N_i) - v(N_j)\|^2}{h^2}} \tag{8}$$

where *h* is the size of the kernel. In this approach, the Euclidean distance $\|.\|$ between two pixels in the bilateral filter [15, 16] is replaced by the weighted Euclidean distance between two patches. Moreover, the Euclidean distance in the weight function is substituted with a Gaussian. Thus, it can be considered as a variation of the neighborhood filter [17].

Wavelet-based Denoising

In wavelet-based denoising, the image is decomposed into subbands (LL, LH, HL, HH) by the wavelet transform as shown in Fig.1. Then, coefficients of the detail subbands are compared with a threshold value and modified ac-

Figure 1. A sample image 'Barbara' and 2-D wavelet decomposition of the image. From top left to bottom right: LL, LH,HL, and HH (detail) subbands.

cording to some thresholding rules. Finally, the image is reconstructed from the updated wavelet coefficients by performing inverse wavelet transform. Generally, there are two thresholding rules: hard-thresholding and soft-thresholding. In hard-thresholding, wavelet coefficients that are smaller than or equal to the threshold value T are set to zero and the others are kept:

$$T_H(x) = \begin{cases} 0, & |x| \le T \\ x, & otherwise \end{cases} \tag{9}$$

On the other hand, in soft thresholding, wavelet coefficients that are larger than the threshold value are shrunk towards to zero by a factor of T:

$$Ts(x) = \begin{cases} 0, & |x| \le T \\ sign(x).(|x| - T), & otherwise \end{cases} \tag{10}$$

Thus, we refer to this latter procedure as the wavelet shrinkage. Here, the signum function *sign*(.) preserves the sign of the wavelet coefficients.

Block-Matching and 3-D Filtering (BM3D)

BM3D is essentially based on Wiener filtering. BM3D clusters the 2-D noisy image patches or blocks that have similar local structures into stacked 3-D groups. Then, a higher dimensional filtering called collaborative filtering is applied to exploit potential similarity between groups. Collaborative filtering reveals the fine details in 3-D groups and preserves the unique features of each group. This filtering operation is realized in three successive steps: 3-D transform of the group, shrinkage of the transform spectrum and the inverse 3-D transform. 3-D transform includes the 2-D transform within a group such as DCT or wavelets and the 1-D transform across groups such as Haar wavelet. Shrinkage by hard-thresholding or wiener filtering is employed to attenuate noise in transform domain. Finally, estimates of grouped fragments are produced by inverting from the transform domain.

Evaluation Criteria

In order to evaluate the performance of the denoising algorithms, we have used two quality metrics: Peak Signal-to-Noise Ratio (PSNR) and Structural Similarity Index Measure (SSIM) [18]. Given a reference image x, the PSNR of the denoised image $\hat{x}$ is defined as:

$$PSNR(x,\hat{x}) = 10log_{10}\left(\frac{255^2}{\|x-\hat{x}\|^2}\right) \tag{11}$$

where $\|.\|^2$ is the $\ell 2$ –norm distance between two images and the SSIM of the image is given by:

$$SSIM(x,\hat{x}) = \frac{(2\mu_x\mu_{\hat{x}}+C_1)(2\sigma_{x\hat{x}}+C_2)}{(\mu_x^2+\mu_{\hat{x}}^2+C_1)(\sigma_x^2+\sigma_{\hat{x}}^2+C_2)} \tag{12}$$

where $\mu_x, \mu_{\hat{x}}$ are the means and $\sigma_x^2, \sigma_{\hat{x}}^2$ are the variances of the images x and $\hat{x}$, respectively, and $\sigma_{x\hat{x}}$ is the covariance of the images. Here, the constant parameters C_1 and C_2 are inserted to stabilize the result in the case that one of the denominator operands is very close to zero.

PSNR metric is merely used for compatibility. SSIM is proven to better represent the image quality [19]. For this reason, we only consider SSIM metric in experimental studies.

RESULTS AND DISCUSSION

For benchmarking purposes, we utilize nine well-known images of size 256-by-256 and 512-by-512 pixels from

Figure 2. Montage of benchmarking images used in the experiments. From left to right and top to bottom: (a) Lena (b) Goldhill (c) Boats (d) Mandrill (e) Cameraman (f) Barbara (g) House (h) Livingroom (i) Pirate.

image set as shown in Fig.2. Images were chosen to represent a categorical set, i.e., human, nature, and textural. AWGN is added to reference images ranging from standard deviation (std) σ=5 to σ=100 with increments of 5 std units.

Robustness

Wiener Filter

In wiener filtering, for a moderate noise level σ = 25, the images were filtered by a NxN kernel ranging from 3 to 13. The results are given in Fig.3. As it can be observed, the optimal wiener filter size was found as 7x7.

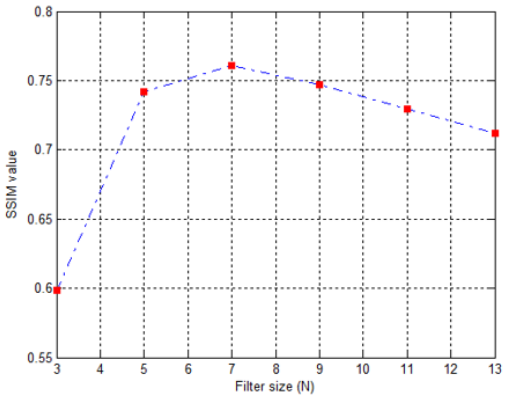

Figure 3. Filter size vs. SSIM value in Wiener filtering.

By increasing noise standard deviation σ = 5 to σ = 100 with 5 units, we denoised the images and superimposed the all results as shown in Fig. 4. It is seen that SSIM value is around 0.73 in σ = 5 case and decreases monotonically towards 0.35 when σ is increased up to 100. It is evident that Wiener filtering is not robust to noise.

Wavelet Hard Threshold

We set up the threshold level to its default value thr = 0.1 and choose a base level of decomposition L =1. The obtained SSIM values for haar wavelet, dual-tree wavelet and double density dual-tree complex wavelet (dddtcwt) [20,21] are 0.289649, 0.320354, and 0.589060, respectively.

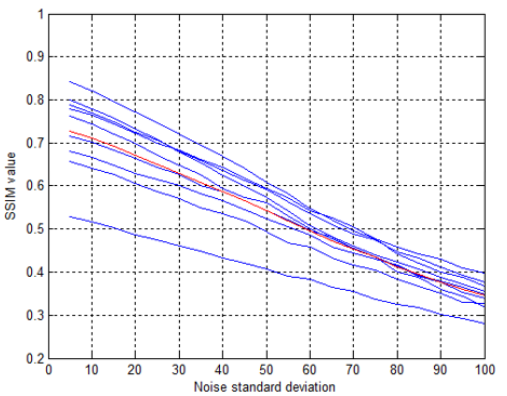

Figure 4. Robustness of Wiener filter (Average is denoted by red curve).

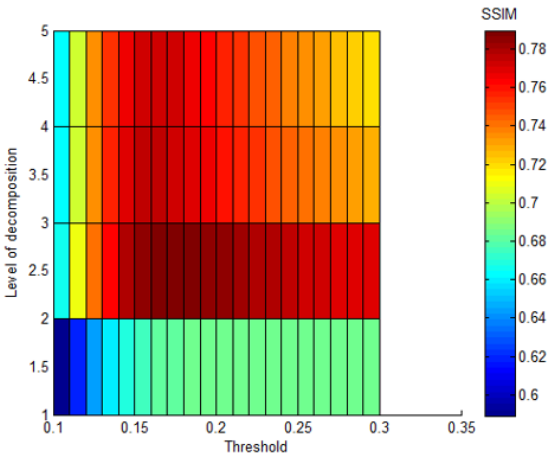

Figure 5. Heat map for optimum values of threshold and level of decomposition for wavelet hard thresholding.

dddtcwt improves the image quality tremendously compared with haar and dual-tree wavelets. Concurrently, we measure the computational burdens of the wavelet types. The average run-time performances are 0.077567, 0.123712, and 0. 0.359911 seconds, respectively, As one would expect, dddtcwt comes with extra computational time which is nearly five times haar wavelet to offer this improved image quality. By setting the wavelet type to dddtcwt, we increase the threshold level from its default value 0.1 with increments 0.01 up to 0.3 and L = 1 to L=5. The more level of decomposition bring out much computational burden. We searched for the optimum values of these parameters and we give the heat map obtained in Fig. 5. It is interesting to note that better SSIM scores are obtained at L=2. The figure demonstrates that as the level of decomposition increases, less peak SSIM scores are obtained. The performance of the algorithm decreases after the decomposition level 2 and saturates after the decomposition level 4. The best SSIM score was achieved at the threshold 0.16 and decomposition level 2 which is 0.7896.

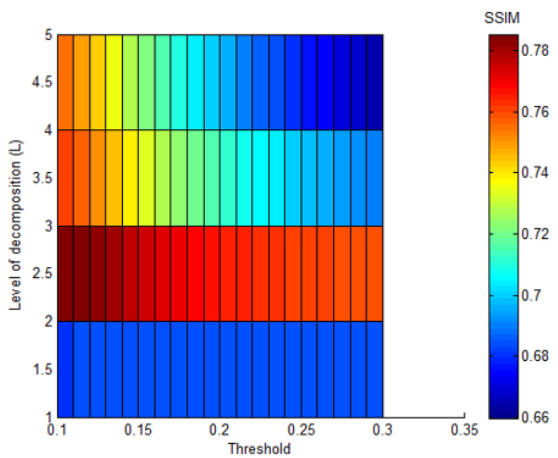

Figure 6. Heat map for optimum values of threshold and level of decomposition for wavelet hard thresholding.

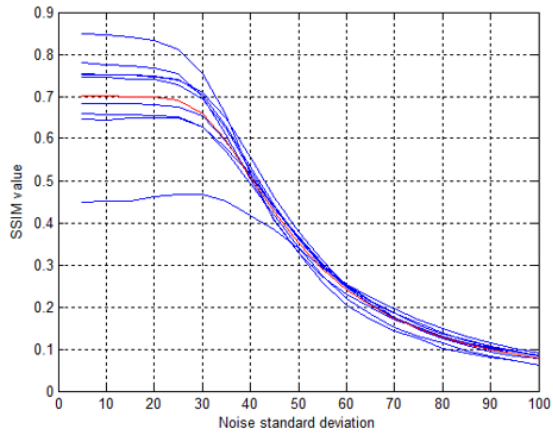

Figure 7. Robustness of wavelet hard thresholding.

Wavelet Soft Threshold

The same procedure was applied for wavelet soft thresholding method. We give the heat map in Fig. 6. As in hard thresholding case, better SSIM scores are obtained at L=2. As the figure demonstrates the performance of the algorithm decreases sharper than hard thresholding after the decomposition level 2. The best SSIM score was achieved at the threshold 0.10 and decomposition level 2 which is 0.7854.

By increasing noise standard deviation $\sigma = 5$ to $\sigma = 100$ with 5 units, we denoised the images and superimposed the results of hard and soft thresholding together as shown in Fig. 7 and Fig. 8. Up to around $\sigma = 30$, the image qualities of both methods are comparable. After $\sigma = 30$, the performances of both methods decrease sharply though soft thresholding gets better SSIM scores. After $\sigma = 50$ for hard thresholding and $\sigma = 60$ for soft thresholding, it is seen that the image qualities of both methods becomes worse than Wiener filtering.

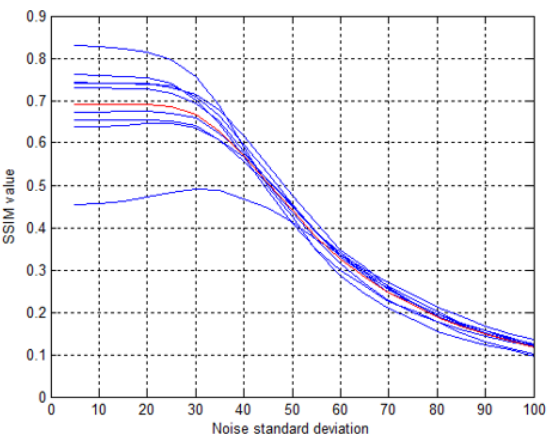

Figure 8. Robustness of wavelet hard thresholding.

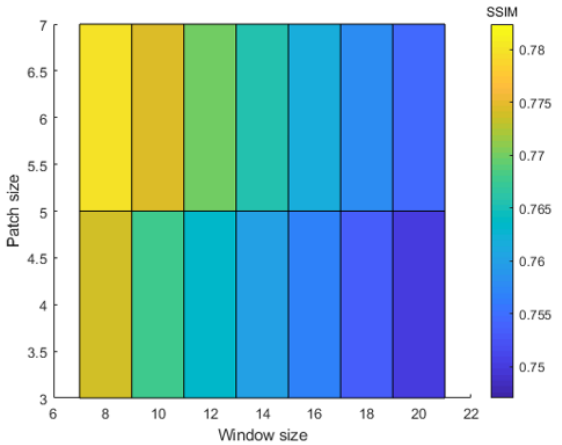

Figure 9. Heat map for optimum values of window size and patch size.

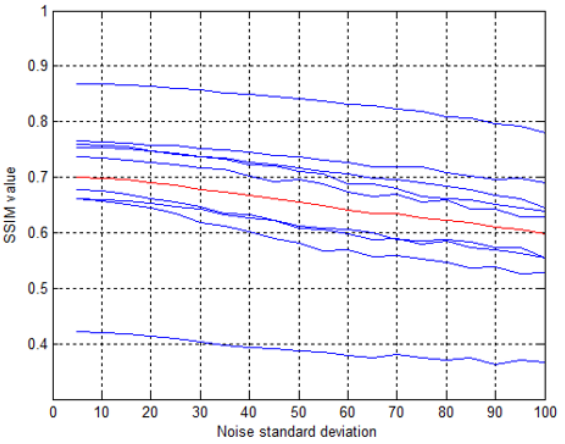

Figure 11. Robustness curve of BM3D.

NLM

In NLM method, as aforementioned two windows are used: patch window and search window. Patch window indicates the neighborhood of the corresponding pixel for weight computations. On the other hand, search window indicates the area wherein similar patches will be searched. In original NLM algorithm, a patch window of the size 7x7 and a search window of the size 21x21 are chosen. But, the search paradigm and suggested values are not suitable for real-world image denoising operations. The original algorithm lasts in time amounts of tens of seconds not milliseconds to complete the denoising task. So, in this study, we preferred to use fast NLM approach [22,23]. The degree of filtering h used in weight computation was chosen as 10 * σ as suggested. As the size of search window increases, the method brings out more computational burden. By varying the patch size in the range 3 to 7 and the window size in the range 7 to 21, we searched for the optimum values of these parameters and obtained the heat map presented in Fig. 9. The figure shows that with a fixed patch size as the window size increases the SSIM scores slightly decreases. Also, with a fixed window size as the patch size increases the SSIM scores slightly increases. Thus, we obtained the best SSIM score with a patch and window size of 7, which is 0.7824.

Fig.10 shows the robustness curve of NLM method. After σ = 25, the performance of the method decreases evidently.

BM3D

It is a well-known fact in very low SNR values, the performance of the BM3D method in terms of image quality deteriorates sharply. There is a quality/complexity trade-off profile selection key in the implementation of the method [24]. Thus, when implementing the BM3D method, we have selected normal profile for balanced quality/complexity. Fig. 11 shows the robustness curve of the method. Although it is observed that the performance decreases slowly, the method is also more robust against noise interference than the prior methods.

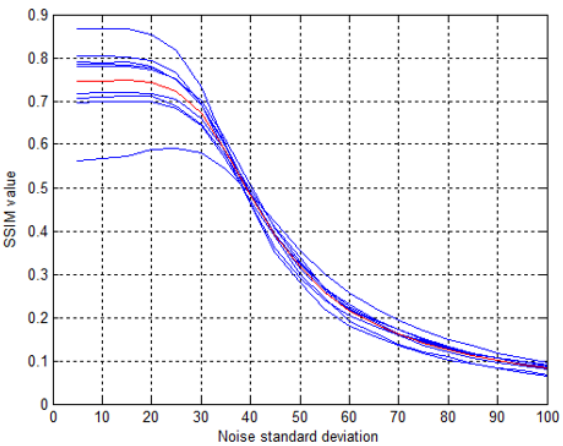

Figure 10. Robustness of the NLM.

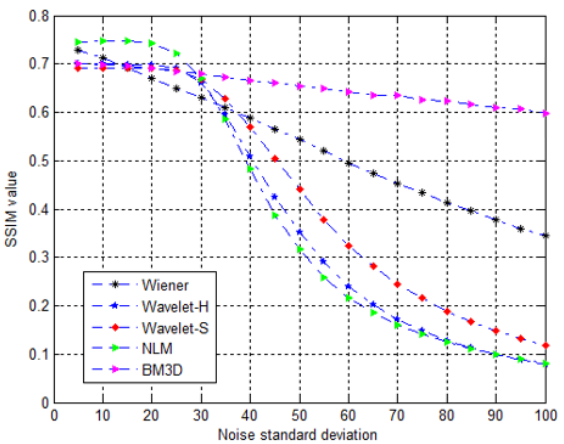

Figure 12. Average robustness of the methods.

Figure 13. Denoised Lena images (σ = 20) (a) Original Lena image (b) Noisy (c) Wiener (d) Wavelet soft thresholding (e) NLM (f) BM3D.

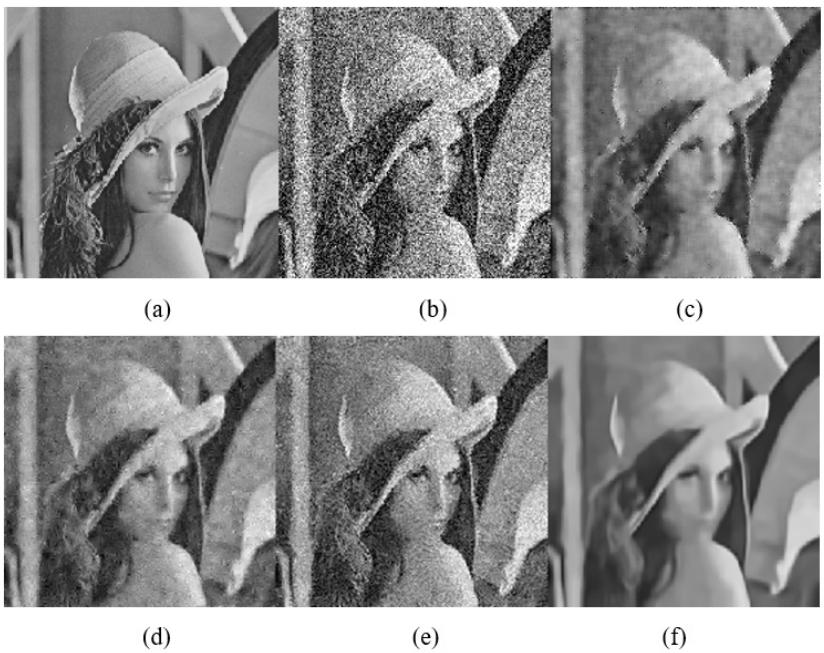

Figure 14. Denoised Lena images (σ = 50) (a) Original Lena image (b) Noisy (c) Wiener (d) Wavelet soft thresholding (e) NLM (f) BM3D.

Denoised Image Quality

Fig. 12 shows the robustness of the methods together averaged over the benchmarking images. As it is observed, BM3D is the most robust method against noise interference. But, at moderate noise levels up to σ = 30, NLM is more robust than BM3D. Moreover, at low noise levels up to σ = 15, Wiener filter performs better BM3D. After σ = 30, the performances of four methods other than BM3D decrease more sharply. It is also interesting to note that Wiener filter performs better than wavelet and NLM methods at moderate and high noise levels after σ = 35.

Fig. 13 and Fig.14 show denoised sample 'Lena' images by Wiener, Wavelet soft thresholding, NLM, and BM3D methods in σ = 20 (low-moderate levels of noise) and σ = 50 (moderate-high levels of noise) cases, respectively.

Table 1. DIQ scores of the methods.

Wiener	Wavelet H	Wavelet S	NLM	BM3D
0.5327	0.3795	0.4230	0.3811	0.6523

Average denoised image quality for each method is calculated by averaging the SSIM values obtained at each σ value of noise interference in the robustness curves over the N benchmarking images. Let the $SSIM_{\sigma}^{i}$ denote the SSIM value of the *i*th image in the dataset obtained at the σ standard deviation of noise interference. Then the average denoised image quality, *DIQ* is given as:

$$DIQ_{Method} = \frac{1}{N}\sum_{i=1}^{i=N}\sum_{\sigma=1}^{\sigma=20} SSIM_{5\sigma}^{i} / 20 \qquad (13)$$

Table 1 shows DIQ scores of the methods. As one would expect, although soft thresholding gets more high denoising score, the performances of both wavelet thresholding methods are quite similar. The denoising score of Wiener filter is remarkable which is higher than the remaining three methods except BM3D.

Computation Time

For a sample image, Table 2 gives the computation times of sizes 256x256 and 512 x512 or when the size is doubled. Experiments were carried out in MATLAB R2018 environment on an Intel Core i5-6200U CPU @ 2.3 GHz computer with 8 GB RAM. The experiments were repeated a hundred times and averaged. If the first case is examined, it can be deduced that Wiener filter is approximately 20x (20 times) faster than Wavelet-based methods, 120x faster than NLM method, and 150x faster than BM3D method. It is observed that NLM and BM3D methods are quite slow with respect to Wiener filter and Wavelet-based methods.

In the second case, when the image size is doubled, this would ideally give 4x extra computational burden. From the computation times it can be deduced that Wiener, Wavelet, and BM3D methods keep their computational burdens in this case. But, NLM cannot keep its computational burden in which case yields 6x extra computational burden.

Fig. 15 shows the DIQ values versus computation times of the respective methods for images of the size 256x256. Optimal algorithms are supposed to have less computational times and at the same time high DIQ scores. According to the figure, Wiener filter satisfies this criterion as much as possible. In this respect, it is observed that NLM is far away from satisfying this criterion.

Table 2. Average computational burdens of the methods (in terms of seconds)

Image size	Wiener	Wavelet H	Wavelet S	NLM	BM3D
256x256	0.0052	0.1081	0.1051	0.6479	0.7863
512x512	0.0181	0.4479	0.4027	3.7751	3.3097

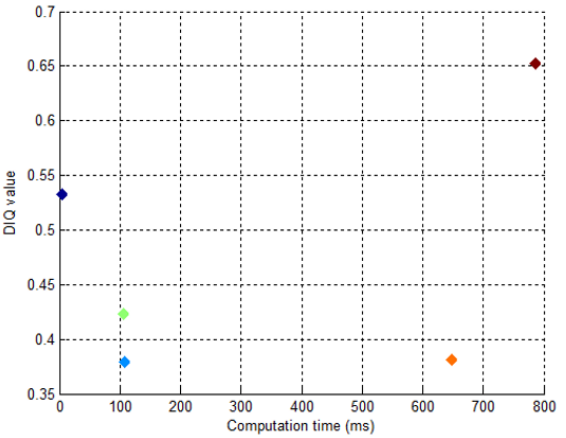

Figure 15. DIQ values versus computation times of the corresponding methods.

CONCLUSION

In time-constrained blind image denoising operations, both image quality and computational burden are important factors. Also, denoising algorithms must be robust to varying noise interference. Due to this, an optimal performance is desired. In this study, we have derived the robustness, image quality, and computational time efficiencies of the image denoising algorithms employed for these goals. From the experimental works, we can conclude that up to moderate noise levels, i.e. σ = 30, NLM is superior to other denoising algorithms, namely, Wiener, Wavelet-based and BMD methods. At high noise levels, especially higher than σ = 50, BM3D performs best in terms of image quality. It is interesting to note that Wiener filter also performs better from Wavelet-based and NLM methods in high noise levels. When the computation times are considered, Wiener filter is far away efficient from the other algorithms. Especially, NLM and BM3D methods are approximately 120x ~ 150x slower than the Wiener filter. We can deduce that under low-moderate noise levels, if the image quality is more important than the computation time NLM can be chosen. Under moderate-high noise levels, if the same goals are required, BM3D is the selection. But, for optimality, Wiener filter is the figure of merit and is considered to satisfy both criterions as much as possible.

CONFLICT OF INTEREST

The authors declare that they have no known competing financial interests or personal relationships that could have appeared to influence the work reported in this paper.

References

1. Yaroslavsky L. Digital Picture Processing. Berlin, Germany: Springer Verlag; 1987.
2. Gonzalez RC, Woods J. Digital Image Processing, 3rd ed. Englewood Cliffs, NJ: Prentice-Hall; 2008.
3. Perona P, Malik J. Scale-space and edge detection using anisotropic diffusion. IEEE Transactions on pattern analysis and machine intelligence. 1990; 12(7): 629-639.
4. Rudin LI, Osher S, Fatemi, E. Nonlinear total variation based noise removal algorithms. Physica D: nonlinear phenomena, 1992; 60(1-4):259-268.
5. Donoho DL, Johnstone IM. Ideal spatial adaptation by wavelet shrinkage. Biometrika, 1994; 81(3): 425-455.
6. Donoho, DL. De-noising by soft-thresholding. IEEE transactions on information theory, 1995; 41(3): 613-627.
7. Chang SG, Yu B,Vetterli M. Adaptive wavelet thresholding for image denoising and compression. IEEE transactions on image processing, 2000; 9(9): 1532-1546.
8. Pizurica A, Philips W, Lemahieu I, Acheroy M. A joint inter-and intrascale statistical model for Bayesian wavelet based image denoising. IEEE Transactions on Image Processing, 2002: 11(5); 545-557.
9. Buades A, Coll B, Morel JM. A non-local algorithm for image denoising. In: 2005 IEEE computer society conference on computer vision and pattern recognition (CVPR'05). 2005 Jun; IEEE: 2; 60-65.
10. Buades A, Coll B, Morel JM. A review of image denoising algorithms, with a new one. Multiscale modeling & simulation, 2005; 4(2): 490-530.
11. Dabov K, Foi A, Katkovnik V, Egiazarian K. Image denoising by sparse 3-D transform-domain collaborative filtering. IEEE Transactions on image processing, 2007; 16(8): 2080-2095.
12. Zhang K, Zuo W, Chen Y, Meng D, Zhang L. Beyond a gaussian denoiser: Residual learning of deep cnn for image denoising. IEEE transactions on image processing, 2017; 26(7): 3142-3155.
13. Goyal B, Dogra A, Agrawal S, Sohi BS, Sharma A. Image denoising review: From classical to state-of-the-art approaches. Information fusion, 2020; 55: 220-244.
14. Bozkurt F, Yaganoglu M, Günay FB. Effective Gaussian blurring process on graphics processing unit with CUDA. International Journal of Machine Learning and Computing, 2015; 5(1): 57.
15. Tomasi C, Manduchi R. Bilateral filtering for gray and color images. In: Sixth international conference on computer vision. 1998 Jan; IEEE: 839-846.
16. Elad M. On the origin of the bilateral filter and ways to improve it. IEEE Transactions on image processing, 2002; 11(10): 1141-1151.
17. Singer A, Shkolnisky Y, Nadler B. Diffusion interpretation of nonlocal neighborhood filters for signal denoising. SIAM Journal on Imaging Sciences, 2009; 2(1): 118-139.
18. Wang Z, Bovik AC, Sheikh HR, Simoncelli EP. Image quality assessment: from error visibility to structural similarity. IEEE transactions on image processing, 2004; 13(4): 600-612.
19. Wang Z, Bovik AC. Mean squared error: Love it or leave it? A new look at signal fidelity measures. IEEE signal processing magazine, 2009; 26(1): 98-117.
20. Sendur L, Selesnick IW. Bivariate shrinkage functions for wavelet-based denoising exploiting interscale dependency. IEEE Transactions on signal processing, 2002; 50(11): 2744-2756.
21. Selesnick I. Wavelet Software at Brooklyn Poly [Internet]. Electrical Engineering: Polytechnic University of New York; [cited: 2023 May 25]. Available from: https://eeweb.engineering.nyu.edu/iselesni/WaveletSoftware/dt2D.html
22. Darbon J, Cunha A, Chan TF, Osher S, Jensen, GJ. Fast nonlocal filtering applied to electron cryomicroscopy. In: 2008 5th IEEE International Symposium on biomedical imaging: from nano to macro. 2008 May; IEEE: 1331-1334.
23. Wu Y. (2023). Fast Non-Local Mean Image Denoising Implementation [Internet]. MATLAB Central File Exchange: Mathworks; 2012 [updated: 2012 Sep 18; cited: 2023 May 25]. Available from: https://www.mathworks.com/matlabcentral/fileexchange/38200-fast-non-local-mean-image-denoising-implementation
24. Foi A. Image and video denoising by sparse 3D transform-domain collaborative filtering [Internet]. Department of Signal Processing: Tampere University of Technology; [cited: 2023 May 25]. Available from: https://webpages.tuni.fi/foi/GCF-BM3D/index.html